THE CELL METHOD FOR POISSON'S EQUATION

by
Stephen V. Harren
http://www.harren.us

0. Contents

1. Governing Equation

Poisson's equation is the simplest second-order partial differential equation, *viz.,*

$$T\nabla^2 u + p = 0\,, \tag{1.1}$$

where u is the transverse displacement of a (*e.g.,* soap) film, p is the upward pressure distribution applied to the film, and T is the surface tension of the film. In rectangular coordinates, the Laplacian is

$$\nabla^2 u = u_{,ii} = u_{,xx} + u_{,yy}\ , \tag{1.2}$$

where the comma denotes differentiation with respect to the spatial coordinates. Also, admissible boundary conditions for eqn. (1.1) are either the displacement u or the outward normal derivative $u_{,n}$ are prescribed at each point of the boundary of the domain.

In polar coordinates we have the Laplacian

$$\nabla^2 u = u_{,rr} + \frac{1}{r}u_{,r} + \frac{1}{r^2}u_{,\theta\theta} \tag{1.3}$$

and the components of the displacement gradient

$$(\boldsymbol{\nabla} u)_r = u_{,r}\ , \qquad (\boldsymbol{\nabla} u)_\theta = \frac{1}{r}u_{,\theta}\ . \tag{1.4}$$

2. Example in Rectangular Coordinates

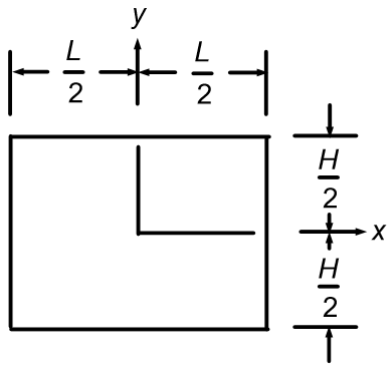

Figure 1. Rectangular domain as described in the text.

At left, in Fig.1, is shown an $L \times H$ rectangular domain subjected to the pressure distribution

$$p = p_0 \cos\left(\frac{\pi x}{L}\right)\cos\left(\frac{\pi y}{H}\right)\ , \tag{2.1}$$

where p_0 is the magnitude of the pressure at the origin. Note that eqn. (2.1) is a "bubble" function, *i.e.,* the pressure is zero on the boundary. The boundary conditions are that u is zero on the boundary. Equation (1.1) may be solved with a displacement of the form

$$u = k \cos\left(\frac{\pi x}{L}\right)\cos\left(\frac{\pi y}{H}\right)\ . \tag{2.2}$$

Note that eqn. (2.2) satisfies the boundary conditions. Notwithstanding, substituting eqns. (2.1) and (2.2) into the governing equation (1.1) yields the value of the constant k, *viz.,*

$$k = \frac{p_0}{\pi^2 T}\left(\frac{L^2 H^2}{L^2 + H^2}\right)\ . \tag{2.3}$$

Also, the displacement gradients are

$$u_{,x} = -k\frac{\pi}{L}\sin\left(\frac{\pi x}{L}\right)\cos\left(\frac{\pi y}{H}\right)\ , \qquad u_{,y} = -k\frac{\pi}{H}\cos\left(\frac{\pi x}{L}\right)\sin\left(\frac{\pi y}{H}\right)\ . \tag{2.4}$$

3. Example in Polar Coordinates

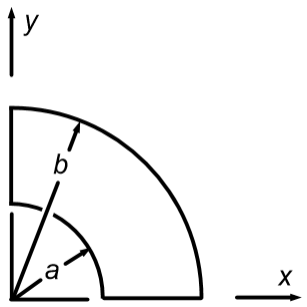

Figure 2. Quarter-annular domain as described in the text.

Figure 2 at left shows a quarter-annular domain subjected to a pressure distribution

$$p = \frac{2F}{b^2 - a^2}\cos\theta \ , \tag{3.1}$$

where F is the net force acting on the domain, *i.e.,* $F = \int_A p\mathrm{d}A$. From eqns. (1.1), (1.3) and (3.1), the governing equation is

$$u_{,rr} + \frac{1}{r}u_{,r} + \frac{1}{r^2}u_{,\theta\theta} = -\frac{2F}{T(b^2 - a^2)}\cos\theta \ . \tag{3.2}$$

The domain is subjected to the boundary conditions $u_{,n} = 0$ on $\theta = 0$ with $u = 0$ on the other three boundaries. Equation (3.2) is solved with a displacement of the form

$$u = f(r)\cos\theta \ , \tag{3.3}$$

which when substituted into eqn. (3.2) yields

$$f'' + \frac{1}{r}f' - \frac{1}{r^2}f = -\frac{2F}{T(b^2 - a^2)} \ . \tag{3.4}$$

The general solution of eqn. (3.4) is

$$f = k_1 r + \frac{k_2}{r} - \frac{2F}{3T(b^2 - a^2)}r^2 \ , \qquad f' = k_1 - \frac{k_2}{r^2} - \frac{4F}{3T(b^2 - a^2)}r \ . \tag{3.5}$$

Consistent with eqn. (3.3), the components of the displacement gradient are

$$(\boldsymbol{\nabla} u)_r = f'(r)\cos\theta \ , \qquad (\boldsymbol{\nabla} u)_\theta = -\frac{1}{r}f(r)\sin\theta \ . \tag{3.6}$$

Looking at eqn. (3.3) and the second of eqns. (3.6), the boundary conditions at $\theta = 0$ and $\theta = \pi/2$ are satisfied identically. Then, satisfying the boundary conditions at $r = a$ and $r = b$ gives the values of the two constants

$$k_1 = \frac{2F(b^3 - a^3)}{3T(b^2 - a^2)^2} \ , \qquad k_2 = -\frac{2Fa^2b^2(b - a)}{3T(b^2 - a^2)^2} \ , \tag{3.7}$$

which two values solve the problem at hand.

4. The Cell Method

What the author calls "The Cell Method" is not a finite element method, nor is it a finite difference method, but perhaps a hybrid of the two. The author just tried this method because it makes sense, and is simple in its idea. Specifically, it is based on the differentiation cell shown below in Fig. 3. The cell spans the normalized domain $\xi_i \in (-1,1)$. Now, with the aid of the quadratic functions

$$f^0(s) = \frac{1}{2}(-s + s^2) \ , \qquad f^1(s) = 1 - s^2 \ , \quad f^2(s) = \frac{1}{2}(s + s^2) \ , \tag{4.1}$$

one may construct the nine interpolation functions S^I via

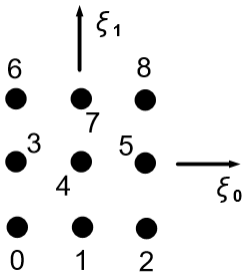

Figure 3. The differentiation cell in normalized **ξ**–space.

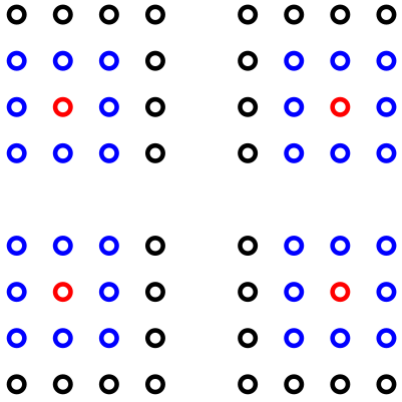

Figure 4. A 4 × 4 computational grid of points containing four differentiation cells.

$$\begin{array}{lll} S^0 = f^0(\xi_0)f^0(\xi_1) & S^1 = f^1(\xi_0)f^0(\xi_1) & S^2 = f^2(\xi_0)f^0(\xi_1) \\ S^3 = f^0(\xi_0)f^1(\xi_1) & S^4 = f^1(\xi_0)f^1(\xi_1) & S^5 = f^2(\xi_0)f^1(\xi_1) \\ S^6 = f^0(\xi_0)f^2(\xi_1) & S^7 = f^1(\xi_0)f^2(\xi_1) & S^8 = f^2(\xi_0)f^2(\xi_1) \end{array} , \tag{4.2}$$

which functions actually are the "shape" functions of the bi-quadratic LaGrange finite element.

The mapping of the differentiation cell to physical **x**–space is achieved via

$$x_i = S^I x_i^I \ , \tag{4.3}$$

where x_i^I are the coordinates of the cell's points. The differentials of eqn. (4.3) are then

$$\mathrm{d}x_i = A_{i\alpha}\mathrm{d}\xi_\alpha \ , \qquad A_{i\alpha} = \frac{\partial x_i}{\partial \xi_\alpha} = S^I_{,\alpha} x_i^I \ , \qquad A_{i\alpha,\beta} = S^I_{,\alpha\beta} x_i^I \ , \tag{4.4}$$

and

$$\mathrm{d}\xi_\alpha = A^{-1}_{\alpha i}\mathrm{d}x_i \ , \qquad A^{-1}_{\alpha i} = \frac{\partial \xi_\alpha}{\partial x_i} \ . \tag{4.5}$$

Now, with the derivative

$$\frac{\partial A^{-1}_{\gamma j}}{\partial \xi_\beta} = -A^{-1}_{\gamma i} A_{i\alpha,\beta} A^{-1}_{\alpha j} \ , \tag{4.6}$$

one finds that the physical gradients of the interpolation functions are, which are obtained via the Chain Rule,

$$S^I_{,j} = S^I_{,\alpha} A^{-1}_{\alpha j} \ , \qquad S^I_{,jk} = \left(S^I_{,\gamma\beta} - S^I_{,\alpha} A_{i\gamma,\beta} A^{-1}_{\alpha i}\right) A^{-1}_{\beta k} A^{-1}_{\gamma j} \ . \tag{4.7}$$

Thus, interpolating the displacement u through the cell using the functions S^I one has

$$u = S^I u^I \ , \qquad u_{,i} = S^I_{,i} u^I \ , \qquad u_{,ij} = S^I_{,ij} u^I \ , \tag{4.8}$$

where u^I are the values of the displacement at the cell's points. In particular, for the Laplacian and normal derivative,

$$\nabla^2 u = S^I_{,ii} u^I \ , \qquad u_{,n} = n_i u_{,i} = n_i S^I_{,i} u^I \ , \tag{4.9}$$

where n_i is the outward-pointing unit normal on the boundary.

Turning attention to Fig. 4 above, the computational procedure of the cell method is as follows.

Figure 4 shows four copies of the same 4×4 computational grid of points. In each copy, in blue and red, are shown the four differentiation cells. Note that the cells overlap. First, at each of the four internal (red) points of the grid, an algebraic equation is constructed by evaluating the governing equation (1.1) at point 4 of each cell (via the operator in the first of eqns. 4.9). Algebraic equations for the remaining 12 points are supplied by the boundary conditions, by either prescribing u or the normal derivative $u_{,n}$ (via the operator in the second of eqns. 4.9). Note that the boundary conditions are applied at either the points 1, 3, 5 or 7 of the cell (unless the boundary point is on a corner, for which the boundary conditions are applied at either the points 0, 2, 6 or 8 of the cell). In any case, a 16×16 system of equations has been constructed, which system may be solved for the 16 nodal displacements.

5. Numerical Example in Rectangular Coordinates

Here the problem solved analytically in Sec. 2 is solved numerically. Due to symmetry, only the upper right quadrant of Fig. 1 needs to be analyzed. The corresponding boundary conditions are

$$u = 0 \text{ on } x = \frac{L}{2} \text{ and } y = \frac{H}{2} \; ; \qquad u_{,n} = 0 \text{ on } x = 0 \text{ and } y = 0 \; . \tag{5.1}$$

The values of the constants used in the analysis are

$$L = 12 \text{ in}, \quad H = 8 \text{ in} \; , \quad T = 4.14 \times 10^{-4} \; \frac{\text{lb}}{\text{in}} \; , \qquad p_0 = 0.005 \; \frac{\text{lb}}{\text{in}^2} \; . \tag{5.2}$$

Note that the value of T is for water.

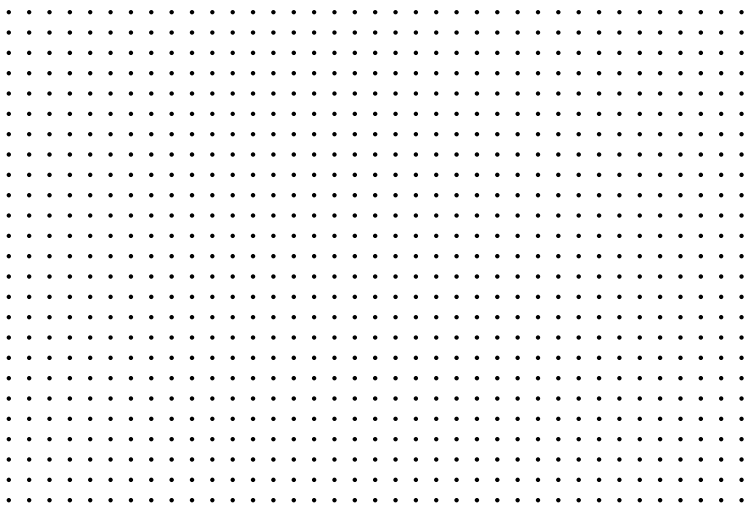

Figure 5. Computational grid used in the analysis.

The computational grid used is shown directly above in Fig. 5. It consists of a 37×25 array of 925 points, and a 35×23 array of 805 overlapping differentiation cells.

In the graphs of the calculated solution shown below in Figs. 6 through 10, the solid curves are from the analytical solution; and the plotted points, from the numerical solution. Looking at the graphs below, the magnitudes of the displacements are very large (which just means that the value used for p_0 in eqn. 5.2 is unrealistically large).

Notwithstanding, the results for the displacement u at the left boundary $x = 0$ are shown below in Fig. 6. As is evident, the numerical results basically coincide with the exact solution. The same thing can be said for the displacement gradient $u_{,y}$ at $x = 0$ (Fig. 7 below).

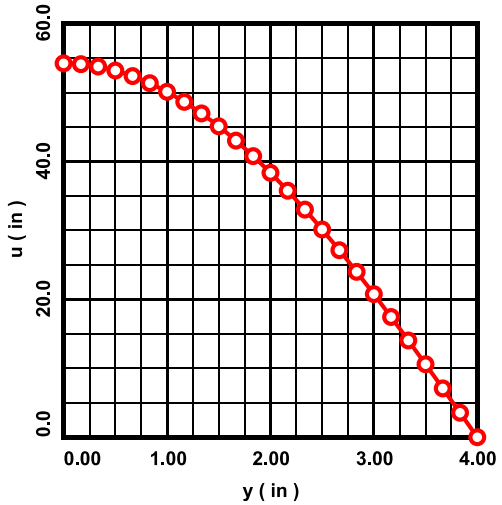

Figure 6. The displacement u at $x = 0$.

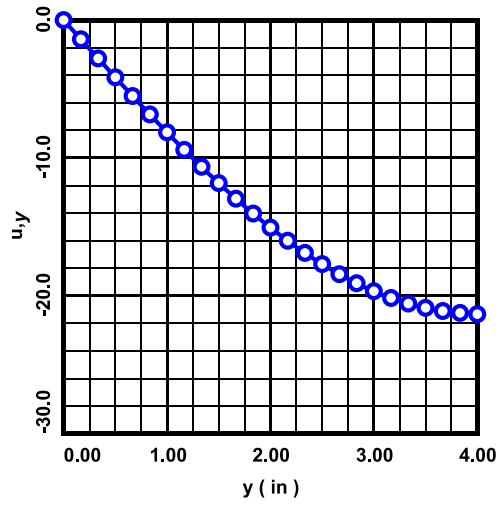

Figure 7. The displacement gradient $u_{,y}$ at $x = 0$.

Figure 8 below shows the displacement gradient $u_{,x}$ at the right boundary $x = L/2$. Once again, the numerically calculated results are highly accurate.

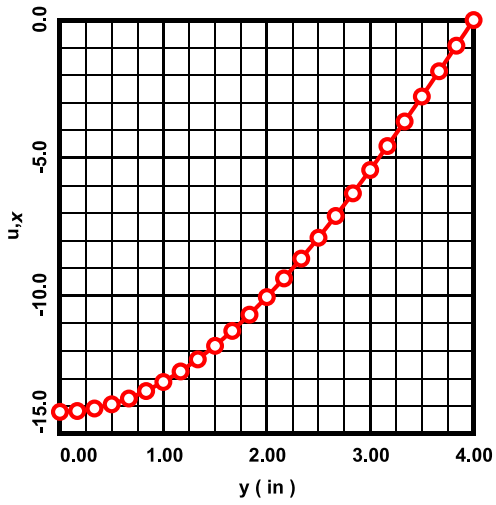

Figure 8. The displacement gradient $u_{,x}$ at $x = L/2$.

Finally, Figs. 9 and 10 below show the results for, respectively, the displacement u, and the displacement gradients $u_{,x}$ and $u_{,y}$ along a vertical line through the grid located at $x = L/4$. As has been the case all along, for all practical purposes, the numerical results correspond to the exact results.

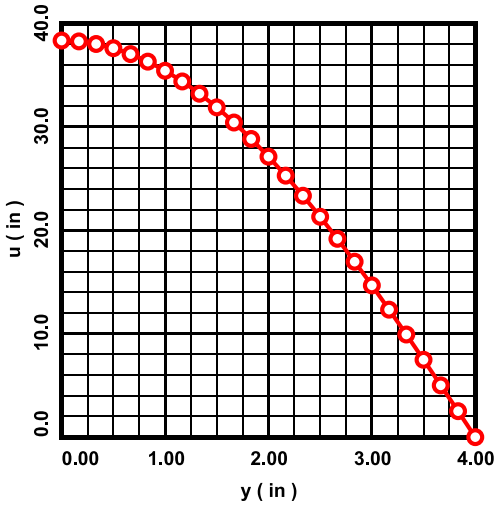

Figure 9. The displacement u at $x = L/4$.

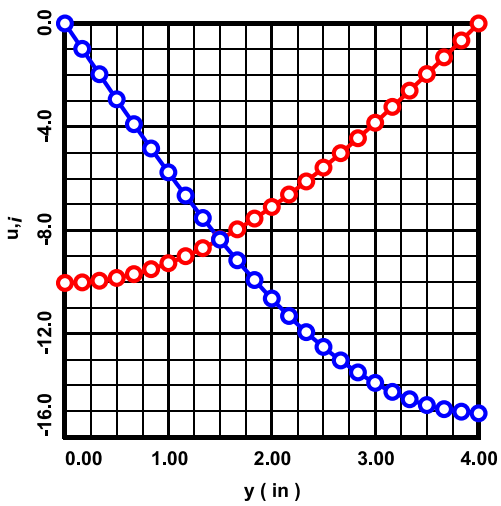

Figure 10. The displacement gradients $u_{,x}$ (red) and $u_{,y}$ (blue) at $x = L/4$.

6. Numerical Example in Polar Coordinates

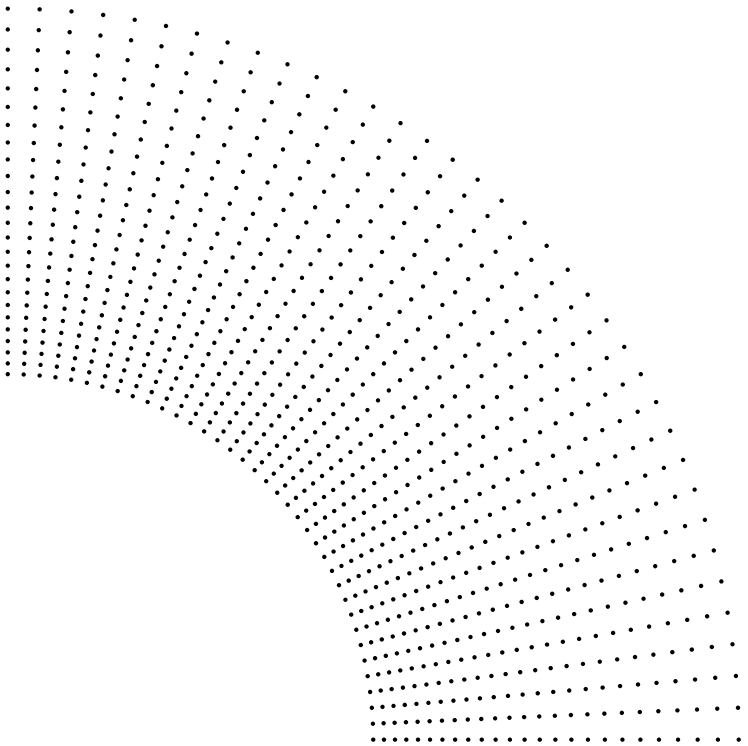

Figure 11. Grid used in the analysis.

Here the problem solved analytically above in Sec. 3 is solved numerically. The grid used in the analysis is shown directly above in Fig. 11. It consists of a 25 (radial) × 37 (tangential) array of 925 points, and a 23 (radial) × 35 (tangential) array of 805 overlapping differentiation cells. The constants used in the analysis are

$$a = 6 \text{ in} \ , \qquad b = 12 \text{ in} \ , \qquad T = 4.14 \times 10^{-4} \ \frac{\text{lb}}{\text{in}} \ , \qquad F = 2 \text{ lb} \ . \tag{6.1}$$

In the graphs of Figs. 12 through 18 below, the solid curves are from the analytical solution; and the plotted points, the numerical solution. As was the case in Sec. 5, here the magnitudes of the displacements are unrealistically high (which just means that the value used for F in eqn. 6.1 is unrealistically large).

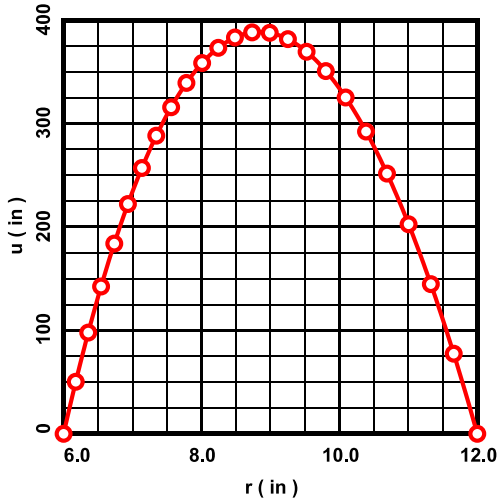

Figure 12. Displacement u at $\theta = 0$.

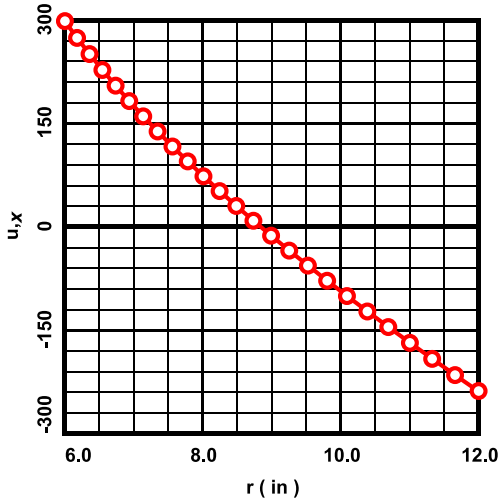

Figure 13. Displacement gradient $u_{,x}$ at $\theta = 0$.

Notwithstanding, the solution along the bottom of the domain at $\theta = 0$ is shown above in Figs. 12 and 13. As is seen, both the calculated displacement u and displacement gradient $u_{,x}$ are highly accurate.

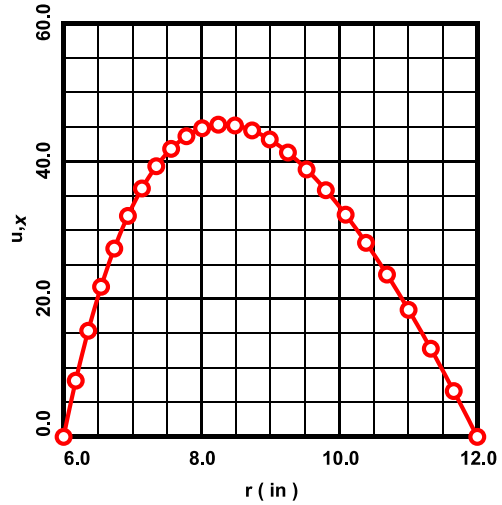

Figure 14. Displacement gradient $u_{,x}$ at $\theta = \pi/2$.

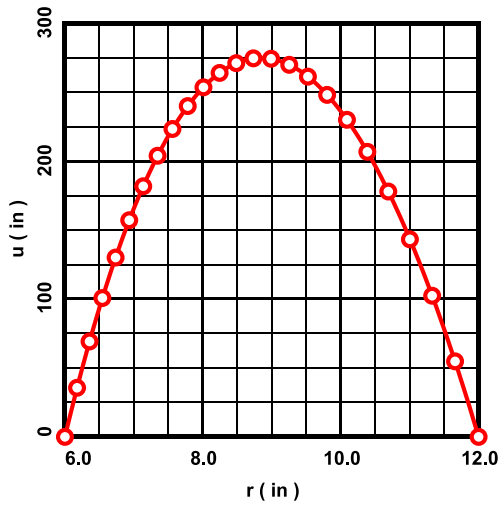

Figure 15. Displacement u at $\theta = \pi/4$.

Figure 14 at above left shows the displacement gradient $u_{,x}$ along the left boundary of the domain at $\theta = \pi/2$. Once again, the numerically calculated solution basically coincides with the exact solution.

Figures 15 (above right) and 16 (below left) show the solution along the radial line of grid points located at $\theta = \pi/4$. As before, the displacement u (Fig. 15) and displacement gradient $u_{,x}$ (Fig. 16) both, for all practical purposes, reproduce the exact solution. Note that at $\theta = \pi/4$, $u_{,x} = u_{,y}$.

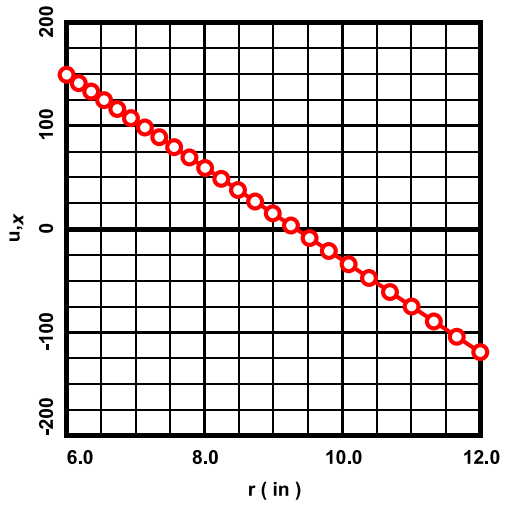

Figure 16. Displacement gradient $u_{,x}$ at $\theta = \pi/4$.

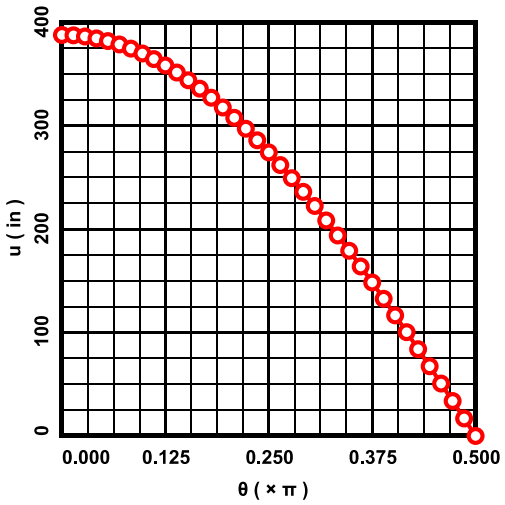

Figure 17. Displacement u at $r = 8.98984$ in.

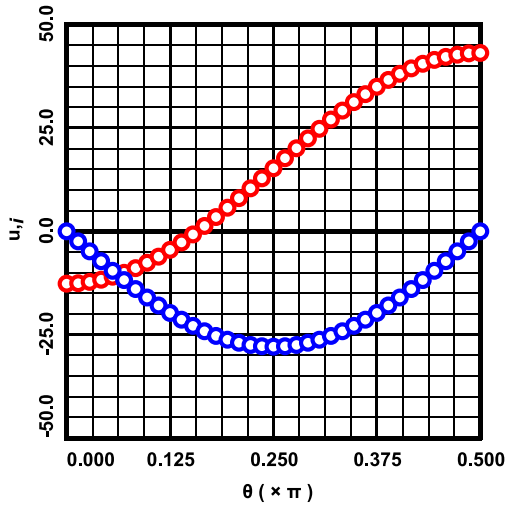

Figure 18. Displacement gradients $u_{,x}$ (red) and $u_{,y}$ (blue) at $r = 8.98984$ in.

Finally, Figs. 17 (above) and 18 (at left) show the numerically calculated solution along the circumferential ring of grid points located at $r = 8.98984$ in. As has been the case all along, the numerically calculated solution is highly accurate.

7. Concluding Remarks

The cell method is perhaps simpler to implement than the finite element method, and the idea behind it is easy to understand. There is not much else to comment on, except that, at least for Poisson's equation, the numerical method yields highly accurate results.